Erschienen in: RSC Advances ; 2 (2012), 12. - S. 5298-5306
https://dx.doi.org/10.1039/C2RA20343J

Biomimetic crystallization of anisotropic zinc oxide nanoparticles in the homogeneous phase: shape control by surface additives applied under thermodynamic or kinetic control†

Carlos Lizandara-Pueyo,[a] Maria Carmen Morant-Miñana,[ab] Martin Wessig,[a] Michael Krumm,[a] Stefan Mecking[a] and Sebastian Polarz*[a]

The bottom-up synthesis of functional materials has become one of the most versatile tools of nanochemistry. It requires not only control over composition and particle size, but also over shape. The fine-control over shape demands an in-depth knowledge about the nucleation and growth of inorganic crystals in the homogeneous phase. A detailed, mechanistic study about the crystallization of zinc oxide is presented here. The findings can easily be transferred to other binary solids with significant ionic character and in particular to those adopting polar crystal classes. New insights about the role of anionic capping agents, cations and kinetic factors during crystallization are reported. One has to conclude that the influence of the cations, specifically the interplay between cation and anion is more significant than expected. Furthermore, low-molecular weight additives containing carboxylic groups are compared to macromolecular additives leading to unusual mesocrystals. Similarities to the concepts of biomineralization are discussed. Finally, a drastic enhancement of photocatalytic activity by several orders of magnitude could be observed for shape-engineered ZnO nanoparticles.

Introduction

The effect of particle shape on functional properties has been highlighted very recently in a number of interesting articles.[1,2] Alterations can be observed for optical, magnetic, catalytic, self-assembly and even toxicological properties. The changes become crucial for high surface to volume ratio. This makes the synthesis and exploration of anisotropic inorganic nanoparticles a contemporary and important task in materials science.

The thermodynamically most stable shape of a crystalline particle (the so-called Wulff shape)[3] is determined by the set of surfaces corresponding to the minimum in total free surface energy. In an ideal case the exposed surfaces relate directly to the planes [hkl] of the underlying crystal lattice. Thus, it follows

$$G_{surf}^{tot} = \sum_{hkl} G_{surf}(hkl) \times A(hkl) \quad (1)$$

with A(hkl) ≅ the surface area of the respective facet. This makes shape inseparably connected to the abundance and type of surfaces.[1] All the more one particular surface dominates the morphology, in other words for highly anisotropic shapes, it can be expected that the properties will differ the most compared to the Wulff shape. Good examples are one-dimensional nanostructures like Xia and Yang illustrate in a stimulating overview.[4]

However, the perception that shape alters (functional) properties is not new. Some of the best examples for the potential behind shape control can be observed in the biological environment.[5] Two examples will be discussed in brief starting with the nano-architecture of the abalone shell nacre.[6] The material is composed of single-crystalline plates of calcium carbonate $CaCO_3$ with interlayered (bio-) polymer domains.[7] This particular architecture enhances the mechanic stability because a force leading to cracks is deflected very effectively.[8] In other words, the shape control for an inferior solid ($CaCO_3$) enables the emergence of superior functionality. The second example involves the creation and application of magnetite nanoparticles for biomagnetism.[9] The Fe_3O_4 nano-crystals exhibit a magnetic moment and enable the organism to navigate within the magnetic field of the earth.[10] The particles are

[a]University of Konstanz, Department of Chemistry, 78457, Konstanz, Germany. E-mail: sebastian.polarz@uni-konstanz.de; Fax: (+49)7531 884406; Tel: (+49)7531 884406
[b]CIC microGUNE (Microtechnologies Cooperative Research Center), Goiru kalea, 9, Polo de Innovación Garaia, 20500, Arrasate, Gipuzkoa, Euskadi.

† Electronic Supplementary Information (ESI) available: ESI-1: Temporal evolution of the anisotropy grade. ESI-2: Influence of the chain length of organic acids on ZnO anisotropy. ESI-3: ZnO prepared in the presence of a PBD additive functionalized with -CH_2CH_3. ESI-4: FT-IR spectroscopy of the material obtained with PBD-COOH-97. ESI-5: PXRD pattern of the ZnO material obtained in the presence of perchlorate ions. ESI-6: Analytical data for ZnO formation in presence of Co^{2+}. ESI-7: Mechanism of the photocatalytic decomposition of Rhodamine B. See DOI: 10.1039/c2ra20343j/

crystallographically oriented with the [111] crystal axis along the chain direction and the particle sizes range typically from 35–120 nm, which is the single-domain-size range for magnetite. It was found that the size and shape of crystals in biominerals is often controlled *via* special biopolymers designed and optimized in the course of biological evolution. The mentioned biopolymers take several actions. Their most important role is the specific interaction and blocking of preferred crystal facets.[11] Mann *et al.* previously reported that the application of the latter principles in materials synthesis bears an enormous potential.[12,13]

In direct comparison, regarding the shape control of man-made nanocrystals, one still stands at the beginning. In accordance to the biomimetic principles that were implied above, the use of capping agents during the nucleation and growth of inorganic particles can strongly affect their morphology.[13,14] The variety of shapes of metallic and ceramic particles is steadily increasing, but often the preparation pathways possess empirical character. The synthesis of anisotropic particles by design is still out of reach because the interplay of thermodynamic, kinetic factors and the effects of capping agents interacting dynamically with the surfaces is very complex. This will be demonstrated in the current article for a material of high contemporary relevance: the wide band-gap semiconductor zinc oxide (ZnO).[15,16] ZnO crystallizes in the Wurtzite structure (space group P_{63mc}) which is a member of the so-called polar crystal classes. As a consequence, it is both pyroelectric and piezoelectric which represents the basis for applications in electromechanical or thermoelectrical coupling devices.[17] This makes the research on anisotropic ZnO nanocrystals a very interesting area.

The effect of differently shaped ZnO nanoparticles on properties and applications could be demonstrated in lasing,[18] photovoltaics,[19] photocatalysis,[20] or UV-blocking.[21] There are several reports on synthetic pathways leading to ZnO nanostructures with high amount of the [002] lattice exposed at the particle surface.[15,21,22,23,24] The capping agents used for the selective stabilization of this crystal lattice are either anions able to coordinate well to Zn^{2+} or polyelectrolytes.[25] Tian *et al.* reported the synthesis of nanoplate-like particles using citrate anions as capping agents.[23] Self-assembly of the particles along the polar [002] surfaces promoted the formation of interesting superstructures. One of the most spectacular results was presented by Wang and co-workers.[26,27] They have prepared so-called nanobelts *via* a gas-phase method. The high exposition of the [002] facet enabled the formation of fascinating nanostructures like the ZnO nanohelices or nanorings.[27] Other interesting morphologies like the nanobell-like and nanopyramid-like shapes have also been reported.[24,28]

In the current contribution we present a comprehensive study in which we try to separate thermodynamic effects, kinetic effects and the effects of anionic as well as cationic additives from each other. The major goal is to derive a detailed knowledge about the factors that determine the evolution of shapes of ZnO nanocrystals during homogeneous nucleation and growth.

Experimental

The preparation of the heterocubane precursors is described elsewhere.[29] All compounds were carefully purified prior to use.

Preparation of ZnO nanoparticles in the homogeneous phase

A typical procedure is as follows. The precursor $[MeZnOtBu]_4$ (0.11 g, 0.18 mmol) is dissolved in dry THF (5 mL). Then one adds the additive (*e.g.* Na-Doc (0.0166 g, 0.075 mmol)) while stirring. After 5 min, the sol–gel process is started by adding water (0.105 mL, 5.83 mmol). The temperature was controlled using a water bath. The dispersion is stirred for further 24 h. Finally the THF is removed by vacuum drying.

Photocatalytic tests

The ZnO particles (50 mg) were dispersed in an aqueous solution of RhB ($c = 2.10^{-5}$ mol l^{-1}; 50 mL). Before irradiation, the dispersion was stirred in the dark for 30 min to establish adsorption–desorption equilibrium at the surface of the catalyst. Then, the mixture was placed at a distance of 10 cm in front of a UV-light source (TQ 150, Heraeus 150 W). Different samples were taken and filtered through a 200 nm syringe filter to remove the ZnO material. The remaining concentration of RhB was determined using UV/Vis spectroscopy.

Characterization methods: FT-IR spectra were measured on a Perkin-Elmer Spectrum 100 spectrometer. The PXRD samples were prepared by removing the solvent from the reaction mixture after 3 days and placing the resulting powder between two Mylar foils. PXRD data were acquired on a Bruker D8 Advance. The TEM and HRTEM samples were prepared by dispersing the particles in THF and adding a drop to carbon foil (Quantifoil-Cu 300 mesh grids). Conventional TEM measurements were performed on a Zeiss Libra 120, high resolution TEM measurements on a Jeol JEM2200FS. UV/Vis spectroscopy was measured on a Cary Variant. EPR measurements at 10 K were performed on a Bruker ELEXSYS E 500 with an ELEXSYS Super High Sensitivity Probe head, cooling down the samples using an Oxford ESR 900 Cryostat, an Oxford ITC 503S was used for temperature control.

Results and discussion

Controlling kinetic factors during crystallization is not an easy task because the rate of nucleation and particle growth can hardly be controlled using simple salt-like precursors like zinc acetate or zinc nitrate. Instead, we have successfully worked for several years with a special molecular precursor system, tetrameric alkylzinc alkoxides $[CH_3ZnOR]_4$ (R = organic group),[30] that allows for the sol–gel preparation of ZnO in organic solvents and enables adjustment of kinetic factors very precisely.[31,32] Furthermore, the advantage of using apolar, organic solvents is that the complexity is reduced because additional interactions with the solvents can be neglected and Ostwald-ripening processes are minimized due to the low solubility of ions in the continuous phase.

First, the growth of particles in the absence of any agent that could specifically interact with the ZnO surfaces was investigated. The ZnO precursor was hydrolyzed using different excesses of water, *f*, while maintaining a constant amount of the precursor. The resulting materials were investigated using transmission electron microscopy (TEM) and powder X-ray diffraction (PXRD) shown in Fig. 1. As expected in all cases one could observe a PXRD pattern that is typical for ZnO in the Wurtzite crystal structure. It is seen that *f* has a significant effect.

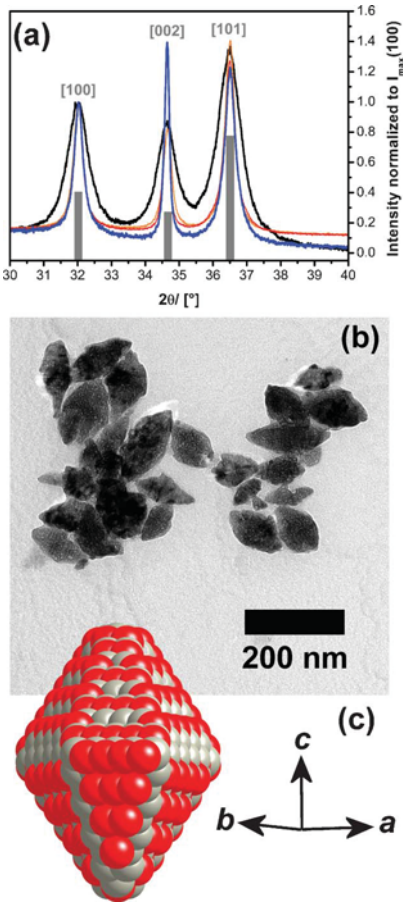

Fig. 1 (a) PXRD of the ZnO materials (reference pattern shown as grey bars) obtained for different amounts of water $f = 1$ (black), 8 (orange), 64 (red) and 128 (blue) at $T = 55$ °C. (b) TEM micrograph and schematic image including the orientation of the crystallographic axes (c) of the particles obtained at $f = 128$.

For the equimolar amount of water ($f = 1$) the single diffraction signals are very broad indicating that the particles have remained small. It is important to note that the signal corresponding to the [002] direction, respective to the length of the particle in crystallographic c-direction is smaller than for the [100] direction which is characteristic for the particle extension in a- and b-directions (see Fig. 1c). The larger f is, the sharper and more intense becomes the [002] signal. This means that the extension of the particles in the c-direction is larger which is in good agreement to the TEM images shown in Fig. 1b. Up to 200 nm long particles with rugby ball-shape are observed. Although the latter morphology (Fig. 1c) looks very interesting, it should be noted that this shape represents the Wulff shape. Thus, it is not very special.

Next, the influence of additives which will interact with the surfaces during growth of the crystals can be checked. But first one has to take into account that the polar [002] lattice plane stand for two surfaces, one composed exclusively of O^{2-} and one composed exclusively of Zn^{2+} ions. Thus it should be possible to address either the zinc terminated surface or the oxygen terminated surface or both.

The role of anionic additives

Organic carboxylates represent good candidates for a potential surface interaction with Zn^{2+}. Therefore, dodecanoate was selected as an additive with Na^+ as a counter-ion (Na-Doc). The resulting nanobell morphology shown in Fig. 2 can be explained by the selective stabilization of the Zn^{2+} terminated [002] interface whereas Na^+ is not suited for the stabilization of the O^{2-} terminated surface. As a consequence, the surface area of the latter is minimized. It is informative to investigate the effect of dodecanoic acid (H-Doc) on the growth of ZnO. It can be clearly seen in the TEM images (Fig. 3a) that the resulting particles possess a morphology differing to those mentioned before. Due to the low intensity and the significant width of the [002] signal in PXRD (Fig. 3b) one can conclude that a nanoplate-like shape (Fig. 3c) has been obtained. The exposure of the polar [002] surface is strongly enhanced. This can only be explained by a significant energetic stabilization of the oxygen terminated surface by protonation as indicated in Fig. 3c. An impression about the kinetics of shape evolution was obtained

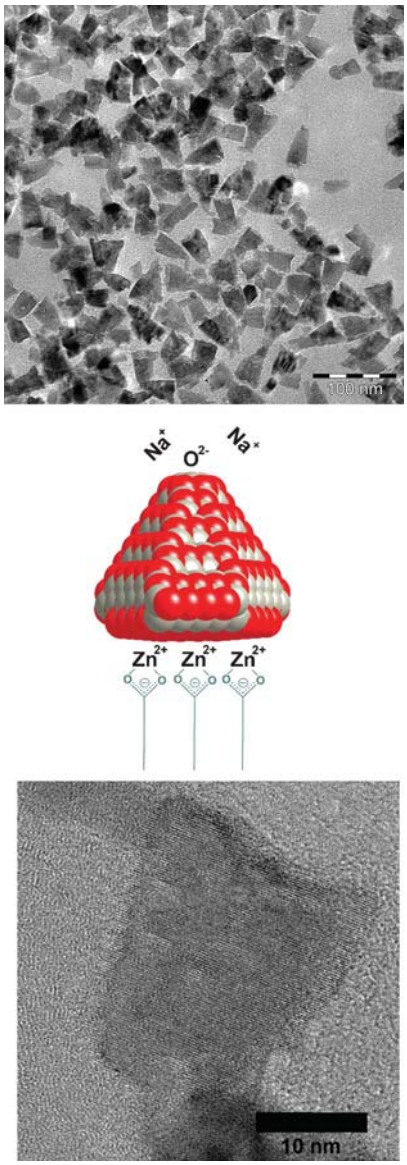

Fig. 2 Effect of an additive interacting specifically with the Zn^{2+} terminated [002] surface in combination with a non-interacting cation. TEM images and scheme of the particle structure.

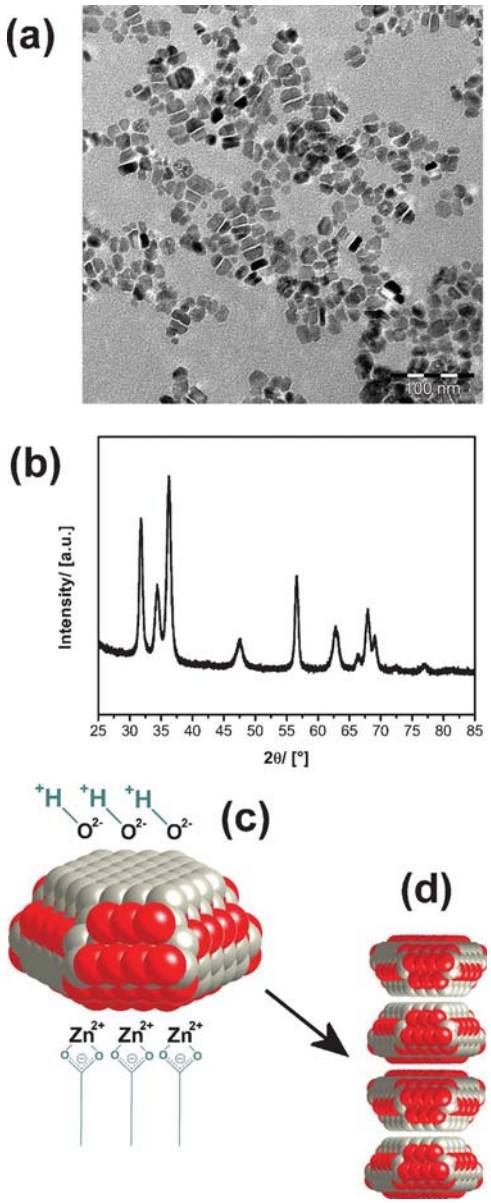

Fig. 3 Nanoplate-like ZnO particles prepared in the presence of dodecanoic acid. (a) TEM, (b) PXRD, (c) schematic image and surface interactions, (d) supercrystal formation.

from taking samples from the dispersion and analyzing them by PXRD. The anisotropy grade defined as

$$R_{aniso} = \frac{D_{a/b}}{D_C} \quad (2)$$

with $D_{a,b,c} \cong$ the extension in a-,b- or c-direction, was calculated and can be plotted as a function of time (see ESI-1†). A spherical nanoparticle would be characterized by $R_{aniso} = 1$, plate-like and [002] rich particles have $R_{aniso} > 1$ and rod-like particles, elongated in the c-direction have $R_{aniso} < 1$. Raniso is ≈ 1 for the first 50 min which is indicative for particles with isotropic shape. Then, during 100–200 min the plate-like shape evolves, followed by a slower anisotropic growth. The hydroxylated surface is still not very stable. Assembly to elongated chains of nanoparticles takes place (Fig. 3a,d).

Before the role of the cation is investigated in further detail, some variations regarding the organic carboxylates should be analyzed. An important question is if only the interaction between surface embedded Zn_{surf}^{2+} and $-COO^-$ is responsible for the stabilization of the respective [002] facet or if the chain length has some influence as well. Therefore, analogous experiments were performed using different organic acids, and the samples were analyzed as before. The resulting correlations are shown in the ESI-2.† It is seen that the length of the alkyl chain attached to the COO^- groups has no impact on particle morphology and also only minor impact on particle size. The colloidal stabilization of the dispersed ZnO nanoparticles is better for longer carboxylic acids because these lead to smaller particle sizes, and a limited tendency for nanocrystal self-assembly (supercrystal formation) can be observed (Fig. 3a).

It was mentioned above that in biomineralization, crystallization is controlled *via* biopolymers which are composed not only of one functional group but contain a large number of them. Because many biopolymers are composed of bifunctional amino acids like aspartic acid or glutamic acid, the carboxylic group has been identified as the most important entity for surface interactions. Thus, it is interesting to study if cooperative effects can occur if additives containing a larger number of –COOH groups interact with the growing ZnO.[33] As a THF-soluble polymer of varying degrees of carboxy-substitution, post-polymerization functionalized polybutadiene was employed (Chart 1). The material was prepared according to ref. 34 by thiol-ene addition of 3-mercatopropionic acid to syndiotactic 1,2-polybutadiene (typically 97% 1,2-content, Mw = 4 × 104 g mol^{-1}, $M_w/M_n = 2$). Degrees of functionalization, that is –COOH groups per butadiene-based repeat unit, amounted to 65%, 85% and 97%, respectively. It should be noted that the PBD macromolecules contain sulfur atoms which could potentially also interact with the ZnO surfaces. Therefore, a blank experiment became necessary before the influence of the carboxylate groups can be studied in detail. A PBD modified with $-CH_2CH_3$ groups was synthesized.[34] The application of the latter resulted in the formation of rugby ball-like ZnO particles (see ESI-3†), and since the latter shape is identical to the Wulff-shape (see above) it is proven that the interaction between the parent polymer and the emerging inorganic phase can be neglected. PBD with different modified degrees of –COOH (65%, 85%, 97%) were prepared and used during crystallization.

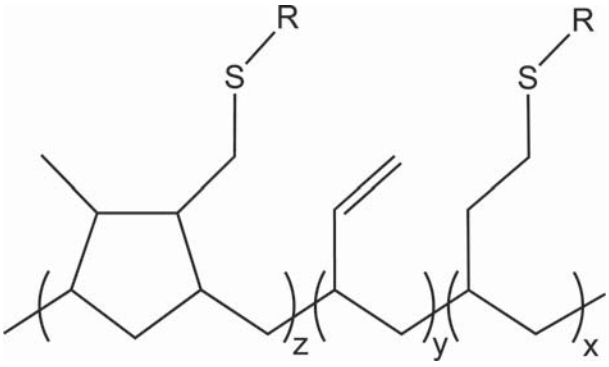

Chart 1 Structure of the used PBD macromolecules. R = $(CH_2)_2COOH$ or $(CH_2)_2CH_3$.

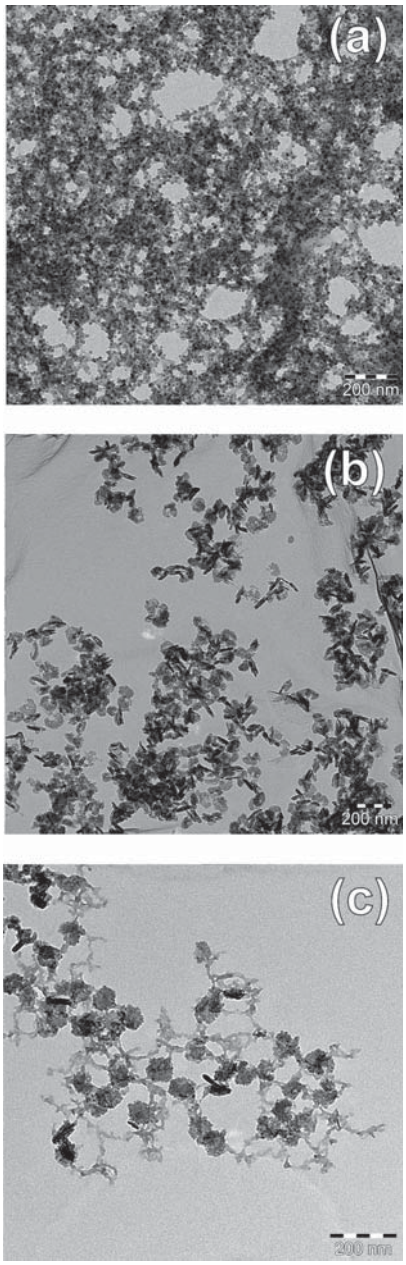

Fig. 4 TEM micrographs of ZnO particles prepared in the presence of carboxylic acid modified PBD macromolecular additives. PBD–COOH-65 (a), PBD–COOH-85 (b) and PBD–COOH-97 (c).

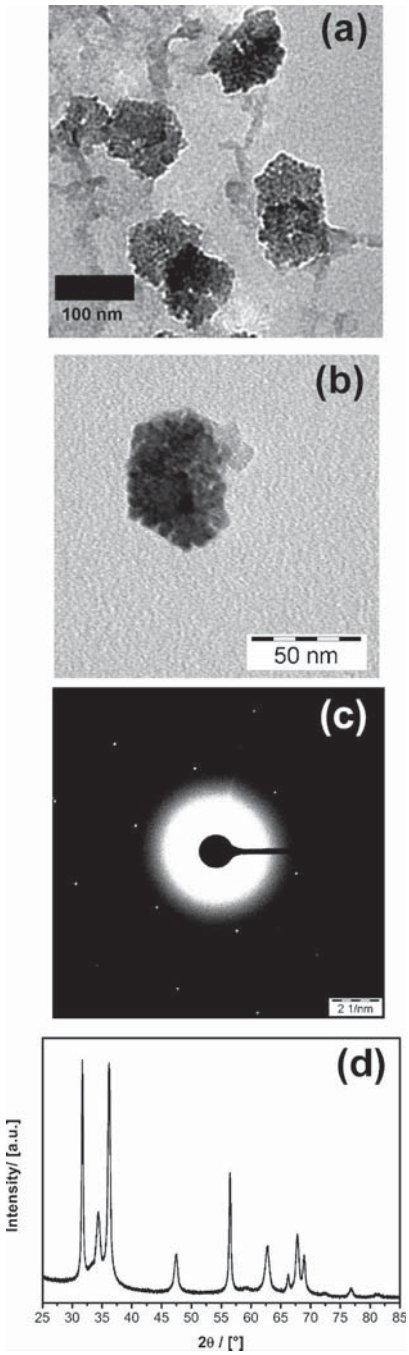

Fig. 5 TEM data for the hexagonal nanoplates prepared with the aid of PBD–COOH-97 shown at two different magnifications (a,b), the single-particle electron diffraction (c) and the PXRD pattern (d).

The results are shown in Fig. 4. Interestingly the polymer with the lowest functionalization degree (PBD–COOH-65) causes the formation of extremely small and almost spherical zinc oxide nanocrystals (Fig. 4a). The product formed using PBD–COOH-85 is very polydispersed regarding size and shape, but some plate-like structures with hexagonal basis can already be seen. Only for PBD–COOH-97 it is found that the majority of the sample consists of these plate-like particles. The latter finding indicates that a high density of interacting groups is essential for an ideal interaction at the organic–inorganic interface. Furthermore, a closer inspection of the TEM images shows that the hexagonal plates are not true single crystals, but are clearly constructed from many even smaller particles with a diameter of $\approx$ 3–5 nm (see Fig. 5a, b). This result seems to be contradicted by PXRD data (Fig. 5d) and electron diffraction. Electron diffraction performed on one particle exhibits a pattern (Fig. 5c) which is typical for a single-crystal with hexagonal symmetry. The [002] signal in PXRD is relatively weak as expected for a plate-like particle, but the width of the diffraction signals corresponds to a crystallite size which is much larger than the primary particle size observed in TEM.

The results can be explained if the very small ZnO nanocrystals self-assemble to a crystallographically oriented,

larger supercrystal (Scheme 1). Crystals with comparable structural features have already been reported for some alternative systems and are believed to also play a key role in biomineralization.[35,36] Due to the involved, non-classical crystallization mechanism, these new class of materials have also been termed mesocrystals.[36,37] However, in comparison to the examples from the literature it should be noted that the mesocrystals found here are the smallest (< 50 nm with primary crystals < 5 nm) that have ever been reported. There was no such self-assembly observed for the long-chain carboxylic acids as additives described above. Therefore, one has to conclude that the polymeric nature in combination with the high density of the functional groups are key for ZnO mesocrystal formation. In addition, it can be proven by FT-IR spectroscopy that all carboxylic groups in PBD–COOH-97 are involved in bonding to the ZnO surface (data are shown in the ESI-4†). The characteristic band for free carboxylic acid (–COOH) at 1705 cm^{-1} has disappeared for the PBD–COOH-97/ZnO nanoparticle composite in favor of a band at 1558 cm^{-1} which is characteristic for coordinating carboxylate (–COO–) functions. The mutual interaction of a multiply carboxylated polymer as a model for PBD–COOH-97 and the zinc terminated [002] surface was simulated using force field calculations with the Materials Studio program package.[38] It was found that there is a high probability for the oriented attachment of the polymer chain caused by the strong binding and the high modification degree of the polymeric additive. The mechanism for the formation of the unusual mesocrystals can be formulated as follows (see also Scheme 1). During the early growth stages PBD–COO^--97 covers the zinc terminated [002] surface while the oxygen terminated surface becomes protonated. Because during these early stages the particle size distribution is expected to be quite monodisperse, we assume that the system lowers its free surface energy further by the fusion of two hydroxylated [002] surfaces. A new building block is formed which has a tightly bound organic, most likely hydrophobic surface at the top and the bottom, and inorganic, polar ZnO surfaces at the sides. The resulting amphiphilic properties induces the oriented self-assembly process. Furthermore, because the interaction along the crystallographic c-axis is dominated by weak van der Waals forces between the organic interfaces, there will be a dynamic equilibrium in solution. This and the patterning of the surfaces due to the oriented attachment of the polymer allows the formation of an equilibrium state in which all primary nanoparticles are precisely oriented to each other (see Scheme 1).

A remaining, open question is if the specific interaction with the zinc terminated [002] surface is limited to carboxylates only. It is worth testing other, multidentate oxygen donors as anionic additives. The generality of the principle can be demonstrated by selecting an anion which is expected to be not very suitable for interaction. The perchlorate anion ClO_4^- belongs to the class of so-called weakly coordinating anions.[39] However, its use during the homogeneous crystallization of ZnO in organic solvents leads to the largest nanoplates and consequently the largest amount of [002] surface we could observe in our study (see Fig. 6; ESI-5†). The latter result shows the enormous potential of crystallizing binary solids in apolar solvents and regarding guiding the interaction between the solid surfaces and the involved additives.

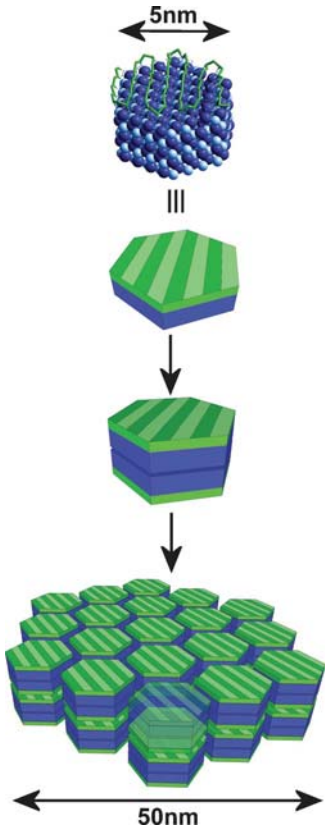

Scheme 1 Stepwise formation of mesocrystals induced by the site specific interaction of carboxylate modified macromolecules (green) with the zinc terminated, polar [002] surface. The inorganic, ZnO parts are plotted in blue in order to highlight the amphiphilic properties.

Particle growth under kinetic control

The reaction rate of ZnO formation can easily be enhanced in various ways. Either a more reactive precursor is used,[31] the concentration of the reactants is amplified, or the temperature is increased. It is very interesting that the particles grown in the presence of Na-Doc behave very differently from the ones prepared with H-Doc. For Na-Doc the nanobell morphology was obtained under thermodynamically controlled conditions (see above). For kinetically controlled conditions, specifically

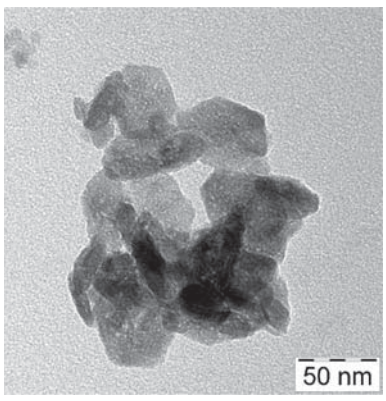

Fig. 6 TEM micrograph of hexagonal ZnO nanoplates prepared with perchlorate anions as structure-directing additives.

high growth rates, one sees that much more elongated, rod-like crystals have formed (Fig. 7a).

Because the particles are stabilized only on one side, apposition on the more or less unblocked surfaces is possible. Furthermore, it is well known that the c-axis, due to the polarity of the [002] plane, is a preferential growth direction (see Scheme 2a). If particle growth occurs even faster, the nanorods have fused together to the star-like aggregates shown in Fig. 7b. The formation of the latter, unusual structures can be explained by considering the influence of defects on crystallization, more specifically multiple twinning (see also Scheme 2b). Twinning has already been recognized for other systems as a major factor influencing morphology.[1,40]

The plate-like morphology emerged because the energy of both polar surfaces, zinc- and oxygen-terminated, was lowered due to effective interactions (see above). This time there is no major change regarding shape if the crystallization is performed under kinetically controlled conditions (see Fig. 7c, d). Because the reaction rate is faster, there will be a higher value for supersaturation in the beginning. It is known from classical nucleation theory that the supersaturation level influences directly the number of critical nuclei.[41] Because for the mentioned conditions more ZnO nuclei form, the final particles remain small after consuming all monomeric species (Fig. 7d).

The previous paragraph points out that the simultaneous control over surface interactions and kinetic factors is of decisive importance for a rational morphosynthesis of metal oxide nanoparticles, shown here for the example of ZnO.

Role of the cation

The effect of a cation exchange from Na^+ to H^+ was already stressed above. Twofold charged cations are also promising candidates for an interaction with the negatively polarized surface. Therefore, cations like Mn^{2+}, Fe^{2+}, Co^{2+}, Ni^{2+}, Cd^{2+}, Hg^{2+} and Ba^{2+} were used. Information about the particle morphology was obtained from PXRD data and TEM. The anisotropy grade R_{aniso} (eqn (2)) was calculated and is plotted as a function of the deviation from the ionic radius of Zn^{2+} (60 pm) Δr in Fig. 8.

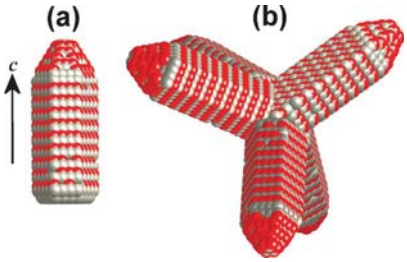

Scheme 2 Schematic representation of the ZnO particles obtained at kinetically controlled conditions (a) and the morphology caused by twinning (b). Surface-bound additives are omitted for clarity.

It can be seen that there is an almost linear relationship. M^{2+} cations with a ionic radius similar to Zn^{2+} bind more strongly to the oxygen terminated surface. This finding indicates that the dominating mode of interaction is electrostatic, unlike to the covalent interaction induced by protonation described before. It can be deduced that Co^{2+} fits best. The successful interaction of Co^{2+} with the surface can be proven by several analytical methods. First, the formation of the ZnO particles was followed by *in situ* UV/Vis spectroscopy measured in transmission mode (data shown in ESI-6†). Unlike the preparation of the pure ZnO particles, there is a significant absorption of light in the Vis region ($\lambda \approx$ 400–500 nm) for the Co^{2+} containing sample. The colour of the initial solution was weak pink and changed within minutes to yellow (see ESI-6†). The yellow colour is a clear indication of the coordination of Co^{2+} to oxygen atoms of the ZnO crystal. The UV/Vis spectra of the resulting particles was also measured. Broad absorption bands between 700 and 550 nm are present (see ESI-6†). The bands match the spectral features reported for ZnO single-crystals doped with Co appearing at

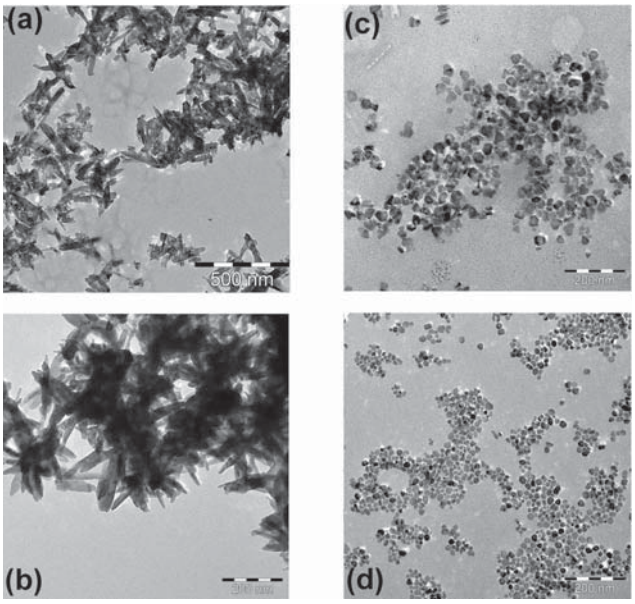

Fig. 7 TEM micrographs of particles grown under kinetically controlled conditions. Particles grown with sodium dodecanoate as an additive under fast (a) and very fast growth conditions (b). Particles grown with dodecanoic acid as an additive under slow (c) and fast growth conditions (d).

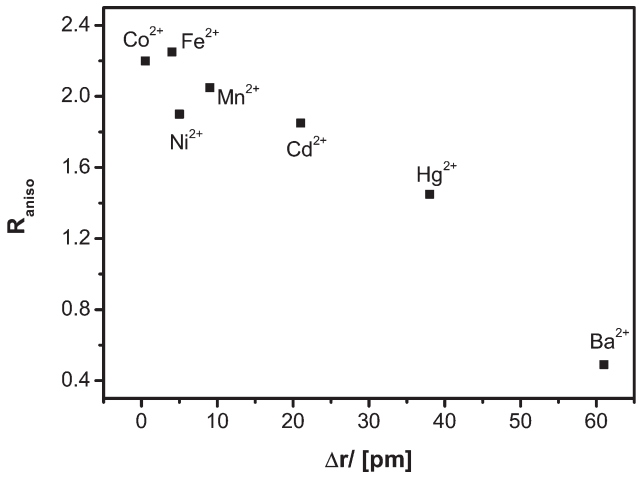

Fig. 8 The anisotropy grade of ZnO nanoparticles prepared in the presence of different cations coordinated to organic carboxylates.

558 nm, 613 nm and 660 nm.[42,43] These results suggest that Co^{2+} occupies Zn^{2+} sites on the surface. Furthermore, EPR measurements were performed at 10 K (see ESI-6†). X-Band EPR spectroscopy allows for the detection of the Co^{2+} species with different coordination geometries. A broad and intense signal between 250 and 5000 Gauss could be seen for the sample synthesized in the presence of Co^{2+}. In agreement to studies on cobalt containing quantum dots, the data can be explained by Co^{2+} existing in an asymmetric, tetrahedral environment.[43] The significant broadening is due to a dipolar coupling caused by the vicinity of the paramagnetic centers on the surface of the ZnO nanocrystals.

Influence of shape on functional properties - photocatalysis

The photocatalytic activity of ZnO was already mentioned in the introduction paragraph of this article.[20] The particles prepared in the current study are ideal to investigate the influence of shape on photocatalytic properties because the materials vary systematically in relative amounts of the polar [002] surface. The photocatalytic decomposition of Rhodamine B (RhB) was selected as a test reaction (see also ESI-7†) and the reaction was followed by time dependent UV/Vis spectroscopy at λ = 555 nm.[44] Using Lambert-Beers law one can easily follow the remaining amount C_{rem} of RhB in solution:

$$C_{rem} = \frac{C(t)}{C_0} = \frac{A_{555}(t)}{A_{555(t=0)}} \quad (3)$$

with $t \cong$ time, $C(t) \cong$ the time dependent RhB concentration, $C_0 \cong$ the RhB concentration at $t = 0$ and $A_{555} \cong$ the absorption value was measured at λ = 555 nm. The materials summarized in Table 1 were used. Entry 1 is a reference sample in which no photocatalyst was presence. There is a very slow photolytic decay (see Fig. 9). For better comparison of the data to each other C_{rem} was fitted by a mono-exponential decay law and the rate constant k was determined (see also Table 1).

$$C_{rem} \propto \exp(-kt) \quad (4)$$

Next, a ZnO material from a commercial supplier with no special morphology and relatively large particles was used (entry 2). It is seen that there is limited photocatalytic activity. ZnO materials comprising isotropic particles and two different particle sizes were prepared. Decreasing the particle size to 16 nm (entry 3) and further to 7 nm (entry 5) results in much better performance due to the increased surface to volume ratio. ZnO nanoparticles with the same extension (16 nm and 7 nm) were synthesized, but the plate-like morphology characterized by

Table 1 ZnO materials used for the photocatalytic tests

Sample number	Shape	Particle Size/[nm]	Rate Constant k/[min-1]
1	—	—	1.65×10^{-4}
2	Isotropic	55	2.82×10^{-3}
3	Isotropic	16	2.38×10^{-2}
4	Nanoplates	16	7.71×10^{-2}
5	Isotropic	7	4.33×10^{-2}
6	Nanoplates	7	2.17×10^{-1}

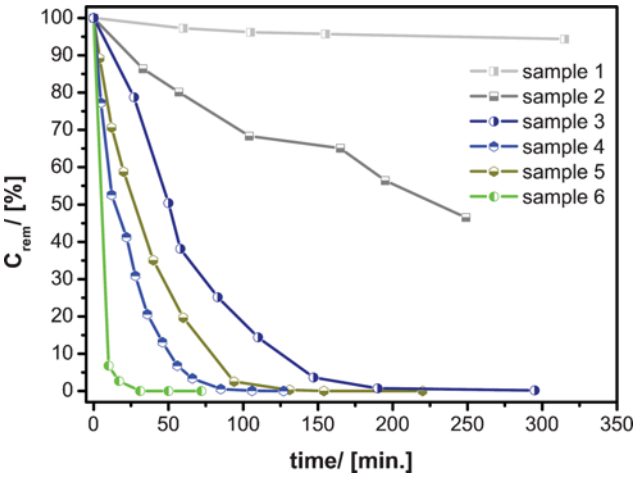

Fig. 9 Photochemical degradation of Rhodamine B using different materials as photocatalysts.

significant amount of the [002] interface were addresses (entries 4 and 6). The direct comparison to the isotropic particles (Table 1) shows that the rate constant is enhanced by a factor of 3–5.

Conclusions

The current paper has described the influence of additives on the homogeneous crystallization of anisotropic ZnO nanocrystals. While most of the recent literature has concentrated almost exclusively on anionic capping agents, here, the eminent importance of cations and their interplay with the anionic additives were explored. The results show the enormous potential of crystallizing binary solids in apolar solvents and the effects of guiding the interaction between the solid surfaces and the involved additives.

It was found that polar surfaces, specifically the [002] surface of ZnO can be addressed separately by anions and cations *via* a specific interactions with the zinc- and oxygen-terminated facets. Thus, the proper choice of a combination of anion and cation is of elemental importance for shape control. Furthermore, it was seen that a similarity in ionic radius in the case of cations and a high density of interacting groups for the anions is essential for an ideal interaction at the organic–inorganic interface. The latter could be demonstrated by comparing low molecular weight carboxylic acids as capping agents to polymers containing high content of carboxylic groups. Although chemically similar, the polymeric additive led to a different and very special morphology. Ultra-small mesocrystals form due to the site specific adsorption on the polar ZnO surface, followed by self-assembly of surface patterned, primary nanocrystals possessing amphiphilic properties (Scheme 1).

Regarding the influence of kinetic factors it was found that an insufficient stabilization of surfaces enhances the effect of fast growth along the main growth directions like the c-axis of ZnO. Even faster reaction kinetics leads to the formation of defects (twinning) which can also strongly affect the morphology of the resulting materials. A kinetic study showed that the formation of particles that differ greatly from the thermodynamically most favoured shape is a relatively slow process.

The crystallization principles described in the current paper can be closely related to the formation of crystalline, inorganic

materials in biominerals. Thus, the concepts presented here can easily be transferred to other binary solids with significant ionic character, in particular if they belong to polar crystal classes. The structures reported here are roughly one length-scale smaller than those in biomineralization, and of course solids of larger technological relevance were prepared. ZnO as a wide band-gap semiconductor compound possesses a range of interesting properties. Its photocatalytic activity was selected here and it could be shown that the rate constant of an exponential decomposition law can be increased by three orders of magnitude by engineering particle shape and size.

Acknowledgements

This work was partly funded by the German Excellence Initiative.

References

1 S. Polarz, *Adv. Funct. Mater.*, 2011, **21**, 3214.
2 (*a*) Y. Xia, Y. J. Xiong, B. Lim and S. E. Skrabalak, *Angew. Chem., Int. Ed.*, 2009, **48**, 60; (*b*) Z. Y. Jiang, Q. Kuang, Z. X. Xie and L. S. Zheng, *Adv. Funct. Mater.*, 2010, **20**, 3634.
3 G. Wulff, *Z. Krysta. Miner.*, 1901, **34**, 449.
4 Y. N. Xia, P. D. Yang, Y. G. Sun, Y. Y. Wu, B. Mayers, B. Gates, Y. D. Yin, F. Kim and Y. Q. Yan, *Adv. Mater.*, 2003, **15**, 353.
5 (*a*) H. A. Lowenstam and S. Weiner, *On Biomineralization*, ed. O. R. Anderson, Oxford University Press, New York, 1989; (*b*) B. S. C. Leadbeater and R. Riding, *Biomineralization in Lower Plants and Animals*, Oxford University Press, Oxford, 1986, vol.**30**, p. 375.
6 (*a*) A. M. Belcher, X. H. Wu, R. J. Christensen, P. K. Hansma, G. D. Stucky and D. E. Morse, *Nature*, 1996, **381**, 56; (*b*) B. L. Smith, T. E. Schaffer, M. Viani, J. B. Thompson, N. A. Frederick, J. Kindt, A. Belcher, G. D. Stucky, D. E. Morse and P. K. Hansma, *Nature*, 1999, **399**, 761; (*c*) F. C. Meldrum, *Int. Mater. Rev.*, 2003, **48**, 187.
7 M. Rousseau, E. Lopez, P. Stempfle, M. Brendle, L. Franke, A. Guette, R. Naslain and X. Bourrat, *Biomaterials*, 2005, **26**, 6254.
8 Q. L. Feng, F. Z. Cui, G. Pu, R. Z. Wang and H. D. Li, *Mater. Sci. Eng., C*, 2000, **11**, 19.
9 (*a*) C. E. Diebel, R. Proksch, C. R. Green, P. Neilson and M. M. Walker, *Nature*, 2000, **406**, 299; (*b*) M. Prenant, *Biol. Rev.*, 1927, **2**, 365.
10 R. B. Frankel and D. A. Bazylinski, *Hyperfine Interact.*, 1994, **90**, 135.
11 J. Aizenberg, J. Hanson, M. Ilan, L. Leiserowitz, T. F. Koetzle, L. Addadi and S. Weiner, *Faseb J.*, 1995, **9**, 262.
12 (*a*) S. Mann and G. A. Ozin, *Nature*, 1996, **382**, 313; (*b*) S. Mann, *Angew. Chem., Int. Ed.*, 2000, **39**, 3393.
13 S. A. Davis, E. Dujardin and S. Mann, *Curr. Opin. Solid State Mater. Sci.*, 2003, **7**, 273.
14 B. Wiley, Y. G. Sun, B. Mayers and Y. N. Xia, *Chem.–Eur. J.*, 2005, **11**, 454.
15 Z. L. Wang, *J. Phys.: Condens. Matter*, 2004, **16**, R829.
16 A. Janotti and C. G. Van de Walle, *Rep. Prog. Phys.*, 2009, **72.**
17 (*a*) D. C. Look, *Mater. Sci. Eng., B*, 2001, **80**, 383; (*b*) F. S. Hickernell, *IEEE Trans. Microwave Theory Tech.*, 1969, **MT17**, 957.
18 M. H. Huang, S. Mao, H. Feick, H. Q. Yan, Y. Y. Wu, H. Kind, E. Weber, R. Russo and P. D. Yang, *Science*, 2001, **292**, 1897.
19 M. Law, L. E. Greene, J. C. Johnson, R. Saykally and P. D. Yang, *Nat. Mater.*, 2005, **4**, 455.
20 E. S. Jang, J.-H. Won, S.-J. Hwang and J.-H. Choy, *Adv. Mater.*, 2006, **18**, 3309.
21 C. Lizandara-Pueyo, S. Siroky, M. R. Wagner, A. Hoffmann, J. S. Reparaz, M. Lehmann and S. Polarz, *Adv. Funct. Mater.*, 2011, **21**, 295.
22 (*a*) T. Xu, X. Zhou, Z. Y. Jiang, Q. Kuang, Z. X. Xie and L. S. Zheng, *Cryst. Growth Des.*, 2009, **9**, 192; (*b*) Z. R. R. Tian, J. A. Voigt, J. Liu, B. McKenzie and M. J. McDermott, *J. Am. Chem. Soc.*, 2002, **124**, 12954; (*c*) C. Pacholski, A. Kornowski and H. Weller, *Angew. Chem., Int. Ed.*, 2002, **41**, 1188; (*d*) Z. Y. Jiang, T. Xu, Z. X. Xie, Z. W. Lin, X. Zhou, X. Xu, R. B. Huang and L. S. Zheng, *J. Phys. Chem. B*, 2005, **109**, 23269; (*e*) J. S. Jeong and J. Y. Lee, *Nanotech.*, **2010**, 21; (*f*) T. Alammar and A.-V. Mudring, *Mater. Lett.*, 2009, **63**, 732.
23 Z. R. R. Tian, J. A. Voigt, J. Liu, B. McKenzie, M. J. McDermott, M. A. Rodriguez, H. Konishi and H. F. Xu, *Nat. Mater.*, 2003, **2**, 821.
24 Y.-P. Du and G. Xie, *CrystEngComm*, 2011, **13**, 437.
25 J. Zhang, H. Liu, Z. Wang, N. Ming, Z. Li and A. S. Biris, *Adv. Funct. Mater.*, 2007, **17**, 3897.
26 Z. W. Pan, Z. R. Dai and Z. L. Wang, *Science*, 2001, **291**, 1947.
27 (*a*) X. Y. Kong, Y. Ding, R. Yang and Z. L. Wang, *Science*, 2004, **303**, 1348; (*b*) P. X. Gao, Y. Ding, W. J. Mai, W. L. Hughes, C. S. Lao and Z. L. Wang, *Science*, 2005, **309**, 1700.
28 (*a*) S. H. Choi, E. G. Kim, J. Park, K. An, N. Lee, S. C. Kim and T. Hyeon, *J. Phys. Chem. B*, 2005, **109**, 14792; (*b*) R. H. Wang, J. H. Xin and X. M. Tao, *Inorg. Chem.*, 2005, **44**, 3926.
29 (*a*) S. Polarz, A. Roy, M. Merz, S. Halm, D. Schröder, L. Schneider, G. Bacher, F. E. Kruis and M. Driess, *Small*, 2005, **1**, 540; (*b*) D. Schroder, H. Schwarz, S. Polarz and M. Driess, *Phys. Chem. Chem. Phys.*, 2005, **7**, 1049.
30 (*a*) M. Krumm, C. L. Pueyo and S. Polarz, *Chem. Mater.*, 2010, **22**, 5129; (*b*) S. Polarz, J. Strunk, V. Ischenko, M. Van den Berg, O. Hinrichsen, M. Muhler and M. Driess, *Angew. Chem.*, 2006, **118**, 3031; (*c*) S. Polarz, F. Neues, M. Van den Berg, W. Grünert and L. Khodeir, *J. Am. Chem. Soc.*, 2005, **127**, 12028; (*d*) V. Ischenko, S. Polarz, D. Grote, V. Stavarache, K. Fink and M. Driess, *Adv. Funct. Mater.*, 2005, **15**, 1945.
31 C. Lizandara-Pueyo, M. van den Berg, A. de Toni, T. Goes and S. Polarz, *J. Am. Chem. Soc.*, 2008, **130**, 16601.
32 C. Lizandara-Pueyo, S. Siroky, S. Landsmann, M. W. E. van den Berg, M. R. Wagner, J. S. Reparaz, A. Hoffmann and S. Polarz, *Chem. Mater.*, 2010, **22**, 4263.
33 U. Schlotterbeck, C. Aymonier, R. Thomann, H. Hofmeister, M. Tromp, W. Richtering and S. Mecking, *Adv. Funct. Mater.*, 2004, **14**, 999.
34 B. Korthals, M. C. Morant-Minana, M. Schmid and S. Mecking, *Macromolecules*, 2010, **43**, 8071.
35 (*a*) M. Mo, J. C. Yu, L. Z. Zhang and S. K. A. Li, *Adv. Mater.*, 2005, **17**, 756; (*b*) Y. Y. Tay, S. Li, F. Boey, Y. H. Cheng and M. H. Liang, *Phys. B*, 2007, **394**, 372; (*c*) J. D. Zhang, J. X. Wang, S. B. Zhou, K. Duan, B. Feng, J. Weng, H. M. Tang and P. Z. Wu, *J. Mater. Chem.*, 2010, **20**, 9798; (*d*) J. B. Liang, S. Bai, Y. S. Zhang, M. Li, W. C. Yu and Y. T. Qian, *J. Phys. Chem. C*, 2007, **111**, 1113; (*e*) C. M. Janet, S. Navaladian, B. Viswanathan, T. K. Varadarajan and R. P. Viswanath, *J. Phys. Chem. C*, 2010, **114**, 2622.
36 M. S. Mo, S. H. Lim, Y. W. Mai, R. K. Zheng and S. P. Ringer, *Adv. Mater.*, 2008, **20**, 339.
37 H. Cölfen and M. Antonietti, *Angew. Chem., Int. Ed.*, 2005, **44**, 5576.
38 *Materials Studio Programm Package*, Accelrys, 5 edn, 2011.
39 (*a*) S. H. Strauss, *Chem. Rev.*, 1993, **93**, 927; (*b*) I. Krossing and I. Raabe, *Angew. Chem., Int. Ed.*, 2004, **43**, 2066.
40 (*a*) J. H. Sun, M. Y. Guan, T. M. Shang, C. L. Gao, Z. Xu and J. M. Zhu, *Cryst. Growth Des.*, 2008, **8**, 906; (*b*) D. J. Smith, A. K. Petfordlong, L. R. Wallenberg and J. O. Bovin, *Science*, 1986, **233**, 872.
41 A. G. Walton, H. Vehkamaki, *Classical Nucleation Theory in Multicomponent Systems*, Springer, 2006.
42 J. J. Freedsman, L. J. Kennedy, R. T. Kumar, G. Sekaran and J. J. Vijaya, *Mater. Res. Bull.*, 2010, **45**, 1481.
43 (*a*) P. Lommens, K. Lambert, F. Loncke, D. De Muynck, T. Balkan, F. Vanhaecke, H. Vrielinck, F. Callens and Z. Hens, *ChemPhysChem*, 2008, **9**, 484; (*b*) P. Lommens, F. Loncke, P. F. Smet, F. Callens, D. Poelman, H. Vrielinck and Z. Hens, *Chem. Mater.*, 2007, **19**, 5576.
44 (*a*) T. Takizawa, T. Watanabe and K. Honda, *J. Phys. Chem.*, 1980, **84**, 51; (*b*) T. Takizawa, T. Watanabe and K. Honda, *J. Phys. Chem.*, 1978, **82**, 1391; (*c*) M. Takahashi, H. Tanida, S. Kawauchi, M. Harada and I. Watanabe, *J. Synchrotron Radiat.*, 1999, **6**, 278; (*d*) X. Y. Liu, B. van den Berg, A. R. A. Zauner and P. Bennema, *J. Phys. Chem. B*, 2000, **104**, 11942.